Spray-assisted assembly of thin-film composite membranes in one process

Spray-assisted assembly of thin-film composite membranes in one process

Shiliang Lin,[a] Yanqiu Zhang, [b] Lu Shao, [b] and Cher Hon Lau [*a]

[a] School of Engineering, University of Edinburgh, Robert Stevenson Road, EH9 3FK, UK. E-mail: cherhon.lau@ed.ac.uk
[b] MIIT Key Laboratory of Critical Materials Technology for New Energy Conversion and Storage, State Key Laboratory of Urban Water Resource and Environment, School of Chemistry and Chemical Engineering, Harbin Institute of Technology, Harbin, 150001, P. R. China

Abstract

Spray coating has been exploited to fabricate and tailor the morphologies of various components in thin film composite membranes separately. For the first time, here we exploit this technology to construct and assemble both the selective layer and porous support of a thin-film composite membrane in a single process. In our approach, spray-assisted non-solvent induced phase inversion and interfacial polymerization reduced the time required to fabricate thin-film composite membranes from 3 – 4 days to 1 day and 40 mins. Our approach did not sacrifice membrane separation performances during desalination of a mixture comprising 2000 ppm of NaCl in water at 4 bar and room temperature. At these conditions, compared to traditional thin film composite membranes, the water permeance of our spray coated membranes was higher by 35.7 %, reaching 2.32 L m^{-2} h^{-1} bar^{-1}, while achieving a NaCl rejection rate of 94.7 %. This demonstrated the feasibility of fabricating thin film composites *via* spray coating in a single process, potentially reducing fabrication time during scale-up production.

Key Words: Thin-film composite membrane, Spray coating, Desalination.

1. Introduction

Water scarcity affects over one-third of the global population [1, 2], and measures implemented to alleviate the stress on our current water supply mostly focus on improving the reuse rate of existing water resources [3, 4]. This is because more than 97 % of water on Earth is seawater [2, 5], which is not suitable for human consumption or utilization in industry. This limitation can be resolved if salts in seawater are separated from each other to produce clean, freshwater i.e., desalination [6]. To date, desalination can be achieved *via* distillation, electrodialysis and membrane separations [7].

Amongst these desalination technologies, membrane separations are considered as the most efficient and can reduce electricity consumption by 78 % when compared to distillation [8]. Since the 1950s, reverse osmosis membranes have been widely used for desalination. However, despite technological advances in reverse osmosis membranes, there remains a trade-off between water permeance vs. salt rejection [9]. A potential solution for resolving this long-standing issue is developing thin film composite (TFC) membranes that comprise a thin, dense selective layer deposited on a porous support layer. Thin selective layers are required to reduce resistance for mass transport of solvent molecules across the polymer film whilst providing a barrier to prevent the transport of dissolved salt molecules [10]. Meanwhile the porous support layer is mainly used to provide mechanical stability to the membrane without impeding water permeance [11].

To construct a TFC desalination membrane, polyethersulfone (PES) is commonly used for the porous support due to its high chemical resistance, mechanical strength and heat stability [12]. Meanwhile selective layers of such membranes mostly comprise polyamide fabricated from the interfacial polymerization of diamines dissolved in water and acyl chlorides dissolved in

organic solvents [13]. In industry, this is typically achieved through dip-coating where a porous support layer is first dipped into a water solution comprising the diamine. Excess diamine is removed from the surface of the porous supporting prior dipping it into an acyl chloride-organic solution [14]. Reactions between the diamine and acyl chloride *via* interfacial polymerization yield a dense polymer layer on top of a porous support. In practice, it may take up to four days to fabricate a TFC membrane (Scheme 1) [15].

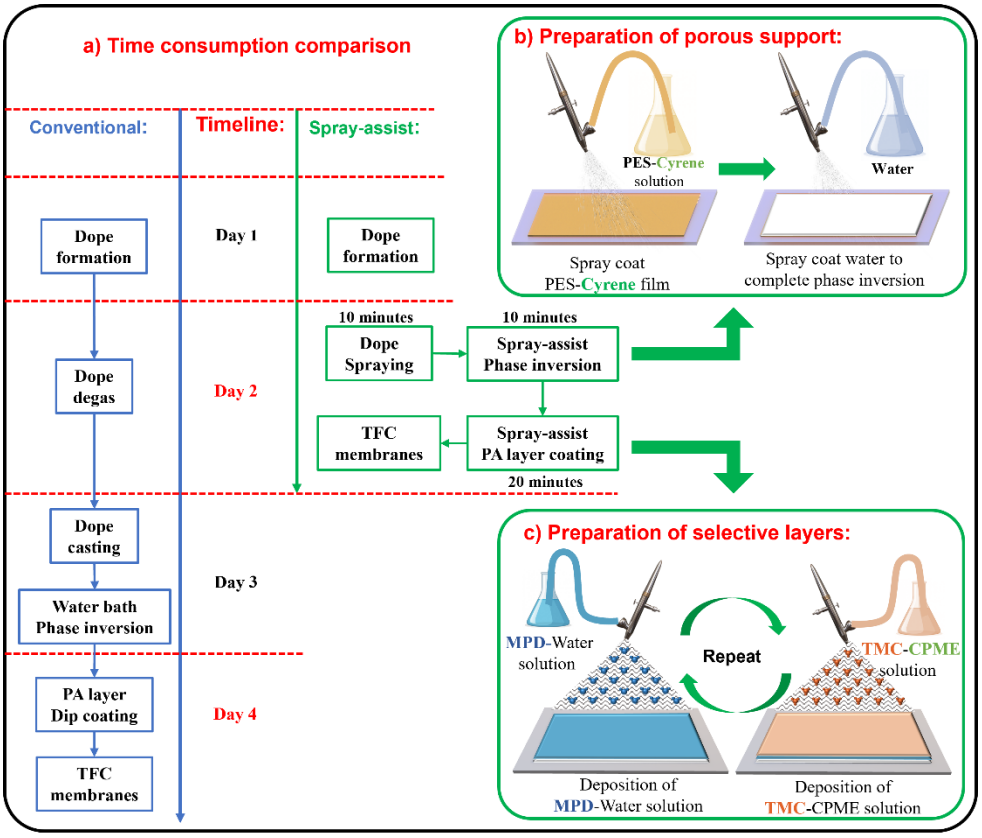

Scheme 1. (a) Timeline comparison between a typical process and our all-in-one spray coating technique developed in this work to fabricate thin film composite membranes. Details for fabricating b) porous support and c) selective layer using spray-assisted non-solvent induced phase inversion and interfacial polymerization, respectively.

The limitation of traditional TFC fabrication methods is that the surface of porous supports cannot dissipate the reaction heat released by exothermic interfacial polymerization reactions in a rapid and uniform manner, leading to the formation of crumpled and thick selective layers that reduce permeability and selectivity [16]. This can be resolved with substrate-free interface polymerization where free-standing, highly crosslinked, 6-nm thin nanofilms with a water

permeance of 2.7 L m^{-2} h^{-1} bar^{-1} has been produced [17]. However, such films are difficult to handle and transfer. This limitation can be overcome by depositing a polydopamine layer on to the surface of the porous support prior polyamide deposition and vacuum treatment [18]. The polydopamine layer functions as an adhesive that ensures robust attachment of polyamide nanofilm on the porous support. Apart from substrate-free interfacial polymerization, TFC membranes can also be fabricated *via* molecular layer-by-layer (mLbL) assembly. This technique requires alternate immersion of a porous support into separate toluene-based solutions containing diamines and acyl chloride until the desired number of mLbL deposition cycle is reached [19]. The water permeance of such membranes 1.48 L m^{-2} h^{-1} bar^{-1}, 2.5-fold higher than those fabricated *via* dip coating, while NaCl rejection rates reached 98.2 % [20]. Despite enabling precise control over polyamide film thickness and roughness, questions remain about the suitability of these fabrication techniques for scale-up production of TFC membranes. This is due to difficulty in handling brittle nanofilms and the complexity of mLbL procedures.

Spray-assisted fabrication techniques such as electrospraying [21], and spray coating [22, 23] offer control over polymerization reaction kinetics and chemistry, membrane morphology and simplicity in material handling. For example, in electrospraying, an electric field is used to distribute amine-water and acyl chloride-hexane droplets, and evaporate the solvents, to form a polyamide selective layer on a porous support layer. Such TFC membranes present a reasonable NaCl rejection of 94 % and a water permeance of 14.7 L m^{-2} h^{-1} bar^{-1} [21]. Such membranes can take up to 120 minutes to fabricate [24], consuming significant energy during fabrication. Different from electrospraying, spray coating enables sequential deposition of reactant solutions on to the substrate. This affords better control over the reaction behavior, whilst reducing fabrication time even during large-scale production [23]. Spraying allows reliable

buildup of homogenous, multi-layered films whilst regulating their thickness and roughness in conditions that are not achievable with dip coating [25]. As such, spray coating is widely used in industry to deposit polymer coatings to yield defect-free thin films as each newly added layer can cover the defects in the previous layers [26].

To date, spray coating has been used to fabricate crosslinked polydimethylsiloxane TFC membranes for ethanol/water separation [27], fluorinated SiO_2 TFC membranes for water/oil emulsion separation [28], carbon nanotube interlayers that enhance the separation performances of a polyamide TFC membrane [29], and polyamide-based TFC membranes *via* a hybrid blade coating-spraying-interfacial polymerization process [30]. We recently also deployed spray coating to fabricate the porous support and using benign, bio-based solvents such as Cyrene™ [31], and using 2-methyltetrahydrofuran (2-MeTHF) and cyclopentyl methyl ether (CPME) to fabricate selective layers of TFC membranes [32]. The separation performances of TFC membranes fabricated from spray-assisted techniques typically surpass those produced from traditional dip coating methods. This demonstrates the potential of fabricating high performance TFC membranes using a well-established industrial technique and common chemicals.

Clearly, spray-assisted techniques are used to fabricate a single component of a TFC membrane. This means that spray coating is usually deployed to produce either the porous support before dip coating is used to deposit the selective layer or to deposit the selective layer on a pre-fabricated porous support layer. Such combinations do not streamline the TFC membrane fabrication process. To date, spray coating has not been deployed to fabricate both the porous support and selective layers in a single process. Here we hypothesize that this knowledge gap can be addressed by enabling both non-solvent induced phase separation (NIPS) and interfacial

polymerization in a single process *via* automated spray coating. In this work, we validated this hypothesis using an automated spray coater developed in our previous works to 1) deposit a PES-Cyrene^{TM} dope solution, 2) enable spray-assisted non-solvent induced phased inversion to fabricate a PES porous support, and 3) drive the interfacial polymerization of trimesoyl chloride and *m*-phenylene diamine on the PES support to fabricate polyamide-based TFC membranes for desalination (Scheme 1). By delivering these mandatory steps for TFC fabrication in a single process, we reduce membrane fabrication duration from 4 days to 1 day and 40 minutes, without affecting membrane separation performances during desalination.

2. Experimental

2.1. Materials

Polyethersulfone (E3020P) was kindly provided by BASF, Germany. Cyrene^{TM} was purchased from Circa Group Ltd, Parkville, Australia. Cyclopentyl methyl ether (CPME), Polyvinylpyrrolidone (PVP, K30) and *m*-phenylenediamine (MPD, >99.5 %) were purchased from Sigma Aldrich. Trimesoyl chloride (TMC, 98+ %) was purchased from Alfa Aesar. n-hexane and ethanol (EtOH, 99.99 % purity) were from Fisher Chemicals.

An automated spray-coating machine adapted from a commercial 3D-printer was used here to fabricate the porous support and selective layers. Details of this machine can be found in our previous work [31]. A Harder & Steenbeck Evolution CRplus Action Airbrush with 0.6 and 0.2 mm nozzle set was purchased from Everything Airbrush, UK. A Creator Pro 3D printer was purchased from FlashForge, China. Servo motors, an Arduino Uno R3 board and connecting cables were purchased from RS Components Ltd, UK.

2.2 Fabricating PES porous supports *via* spray coating

PES dope solutions were prepared by dissolving 15 wt.% PES and 1 wt.% PVP i.e., porogen in Cyrene™ at 80 °C. This dope solution was stirred magnetically until complete PES dissolution, forming a viscous and transparent solution. This process took place over 24 hours to ensure full dissolution of the PES [33-37]. This dope solution was loaded into the solution reservoir of a spray gun with a 0.6 mm nozzle set installed inside. Spraying distance was set to 20 cm above a glass plate (15 cm x 23 cm) placed on the build plate of the 3D printer. The build plate Building plate was set at 20 °C throughout spray coating. 4 bar of nitrogen was supplied to the spray gun and spray gun movement was controlled by the control circuit and stepper motors [31]. The spray gun moved across the glass plate to ensure full coverage of the printing area. This process was repeated for 6 times at room temperature to produce a PES-Cyrene film with thickness around 200 μm. After the dope solution was deposited on top of a glass plate, deionized water was deposited over 5 cycles on to the wet PES-Cyrene film *via* spray coating using 4 bars of nitrogen. The PES film was allowed to rest for 10 minutes for solvent exchange between water and Cyrene to take place. Excessive water on the surface of the coagulated PES membrane was drained away. The resultant PES membrane was then used as a porous support for TFC membranes.

2.3 Conventional fabrication of polyamide selective layers

2 wt.% of MPD was dissolved in water to form the water phase solution and 0.2 wt.% of TMC was dissolved in n-hexane to form the organic phase solution. A PES porous support fabricated from the method outlined in Section 2.2 was taped to a glass plate, with the top surface facing upwards. This porous support was placed in the MPD-water solution for 5 minutes. The amine-loaded PES support was removed from the solution and pressed with a roller to remove excess amine solution, prior immersion in the TMC-n-hexane solution. After 5 minutes of immersion in organic solution, the TFC membrane was placed in a 50 °C oven for 5 mins to allow the

interfacial polymerization to complete and washed with n-hexane and water to remove unreacted monomers. This polyamide TFC was used for control experiments that yielded data required for benchmarking the separation performances of other membranes developed in this work. As such, we named this membrane, Polyamide-PES TFC (dip coating).

2.4 Spray-assisted fabrication of polyamide-PES TFC membrane

Due to the neurotoxicity of n-hexane and health and safety reasons [38, 39], we did not use the spray-assisted technique to fabricate TFC membranes using n-hexane. Instead, we used spray coating to deposit CPME solutions containing trimesoyl chloride. 2 wt.% of MPD was dissolved in water to form the water phase solution, and 3 wt.% TMC was dissolved in CPME to form the organic phase solution. As shown in our previous work, a higher concentration of TMC is required to form dense polyamide selective layers when CPME is deployed as a solvent [32]. This is attributed to the slight water miscibility of CPME affecting MPD diffusion behavior in the CPME-water interface [40-42].

The MPD-water and TMC-CPME solutions were loaded into the reservoir of two separate spray guns with 0.2 mm nozzles, respectively. Without changing the spraying pressure (4 bar) and spraying path, the MPD-water solution was first deposited on top of the PES support (30 seconds). Subsequently the TMC-CPME solution was deposited on top of the thin layer of MPD-water solution (30 seconds) and allowed to rest for 30 seconds. This 30-second rest period is required to allow interfacial polymerization to take place and form a polyamide thin film. These steps constitute to one spray cycle that lasted for 90 seconds (60 seconds of spraying and 30 seconds of rest time). This cycle was repeated for up to 5 times. Thereafter, the entire glass plate was placed inside a 50 °C oven for 5 mins to allow the interfacial polymerization to complete. The resultant TFC membranes were then stored in a deionized water bath prior to

further characterization. Depending on the number of spray cycles, here we named these spray-coated membranes as Polyamide-PES TFC (spray coating - 1 cycle) to Polyamide-PES TFC (spray coating - 5 cycles).

2.5 Membrane characterizations.

The skin layer and cross-section morphologies of membrane samples studied here were observed with a Carl Zeiss SIGMA HD VP Field Emission Scanning Electron Microscopy (FE-SEM). All samples were dried for 12 h in a vacuum oven before SEM analysis. For cross-section SEM characterization, membrane samples were first freeze-fractured in liquid nitrogen. A 10 nm-thin layer of gold was sputter-coated on to the samples before imaging. An accelerating voltage of 5 kV was used to obtain SEM micrographs.

Fourier transform infrared spectroscopy (FTIR) was performed in attenuated total reflectance (ATR) mode on a Nicolet™ iS™ 20 FTIR Spectrometer (Thermo Scientific™) with a Smart iTX™ diamond accessory to characterize functional groups over a range of 500 ~ 4000 cm^{-1}. XPS Analysis was performed using a Kratos Axis SUPRA XPS fitted with a monochromated Al kα X-ray source (1486.7 eV), a spherical sector analyzer and 3 multichannel resistive plate, 128 channel delay line detectors. All data was recorded at 150 W and a spot size of 700 µm x 300 µm. Survey scans were recorded at a pass energy of 160 eV, and high-resolution scans recorded at a pass energy of 20 eV. Electronic charge neutralization was achieved using a magnetic immersion lens. Filament current = 0.27 amp, charge balance = 3.3 volts, filament bias = 3.8 volts. All sample data was recorded at a pressure below 10^{-8} Torr and at 150 K temperature. Data was analyzed using CasaXPS v2.3.20PR1.0 and the spectra were calibrated with C1s peak at 284.8 eV. Each PA sample's Atom% was calculated using the CasaXPS

software and the crosslinking degree in each type of polyamide was calculated using the following equations:

$$\frac{O}{N} = \frac{3m + 4n}{3m + 2n} \qquad (1)$$

$$m + n = 1 \qquad (2)$$

$$Crosslinking\ degree = \frac{m}{m + n} \qquad (3)$$

where O/N is the atomic ratio of polyamide, m and n are the portion of crosslinked and linear parts. All samples were dried for 12 h in a vacuum oven before analysis. AFM topography images of the PES support and polyamide TFC membranes were obtained using a Nanoscope IIIa Multimode scanning probe microscope (Bruker AXS Inc) with an E-scanner in tapping mode using silicon cantilevers. No other image processing was applied except flattening, which was performed here using Gwyddion.

2.6 TFC membranes desalination test.

The water permeances of the PES and TFC membranes were measured using triplicate samples and a Sterlitech stainless steel HP4750 stirred dead-end cell. The feed solution comprised deionized water obtained from a lab-based water purification system and pressurized with nitrogen gas at 1 bar at room temperature to reach steady flow rate, then measured at 3 bars. During filtration, the feed solution was stirred at 400 rpm. Permeate samples were collected in capped flasks as a function of time, weighed, and analyzed. The permeance was calculated using the following equation:

$$Permeance = \frac{V}{At\Delta P} \qquad (4)$$

where permeance ($L \bullet m^{-2} \bullet h^{-1} \bullet bar^{-1}$) is expressed in terms of V, the volume of the solvent passing through the membrane (L), A – effective membrane area (m^2), t – operation time (h), and ΔP – the applied pressure (bar).

The salt rejection rates of TFC membranes were determined using a 2000 ppm NaCl water solution as feed solution and stirred at 400 rpm to avoid concentration polarization. The feed solution was pressurized at 3 bar to reach a steady flow rate and measured at 3 bars. The feed and permeate salt concentrations were determined by measuring water conductivities with a Thermo Scientific Orion Star A212 benchtop Conductivity Meter. Rejection rates of the TFC membranes were calculated using the following equation (5):

$$Rejection\ rate = \left(1 - \frac{C_p}{C_f}\right) * 100 \qquad (5)$$

where C_p and C_f are the solute concentrations in the permeate and feed solution, respectively.

3. Results and discussions.

3.1 PES support layers from spray-assisted NIPS

PES support layers are usually fabricated over 2 – 3 days where a dope solution is formulated by stirring/mixing to ensure full dissolution of the PES [33, 34], followed by a degas step that could take up to 24 hours for releasing air bubbles trapped inside the viscous dope solution [34-37]. Upon degassing, the well-rested dope solution is then cast into a wet PES film. This wet film is then immersed in a water bath for 24 hours to enable polymer coagulation whilst ensuring complete solvent exchange [34, 37, 43, 44].

Here we halved this time-consuming fabrication protocol using our spray-assist technique. In our approach, we used the same time as per the traditional method (24 hours) to formulate the dope solution. However, we obviated the degas step in our protocol as air bubbles could still be encapsulated in the dope solution droplets during spray coating, this has been shown in our previous work [31]. We loaded this dope solution into a spray gun and used 4 bar of nitrogen

to break up this viscous solution into droplets that were deposited on top of a glass plate, yielding a PES-Cyrene wet film in 10 minutes. Once this wet film was formed, we deployed spray-assisted NIPS over 5 cycles of water deposition to enable polymer coagulation within 10 mins (Scheme 1). Our approach to fabricate PES support layers in this work is different from our previous protocol [31].

When compared to PES support layers that coagulated in a water bath (conventional method), the surface of our spray-assisted PES porous support layer reported here was more porous (Fig. 1a – b). This increase in surface porosity due to spray coating was also observed elsewhere where spray-coated water droplets enabled a more instantaneous/faster inversion process that leads to the formation of more porous membranes [45]. We also observed that phase inversion achieved through spray-coated water droplets also led to the formation of membranes with a sponge-like structure at the bottom side and shorter finger-like pores at the top cross-section, when compared to membranes produced *via* a phase inversion process over water immersion. This was similar to observations reported elsewhere [46]. The surface and cross-sectional morphologies of PES membranes that were fabricated with three to five spray-assisted water deposition were similar (Fig. S1). This indicated that NIPS process was completed after three water deposition cycles. Meanwhile additional water deposition cycles were required for complete removal of residue Cyrene. The pure water permeance of PES support layers fabricated *via* spray-assisted NIPS was 135.65 L m^{-2} h^{-1} bar^{-1}, 2-fold higher than PES support layers fabricated using Cyrene and water immersion [31].

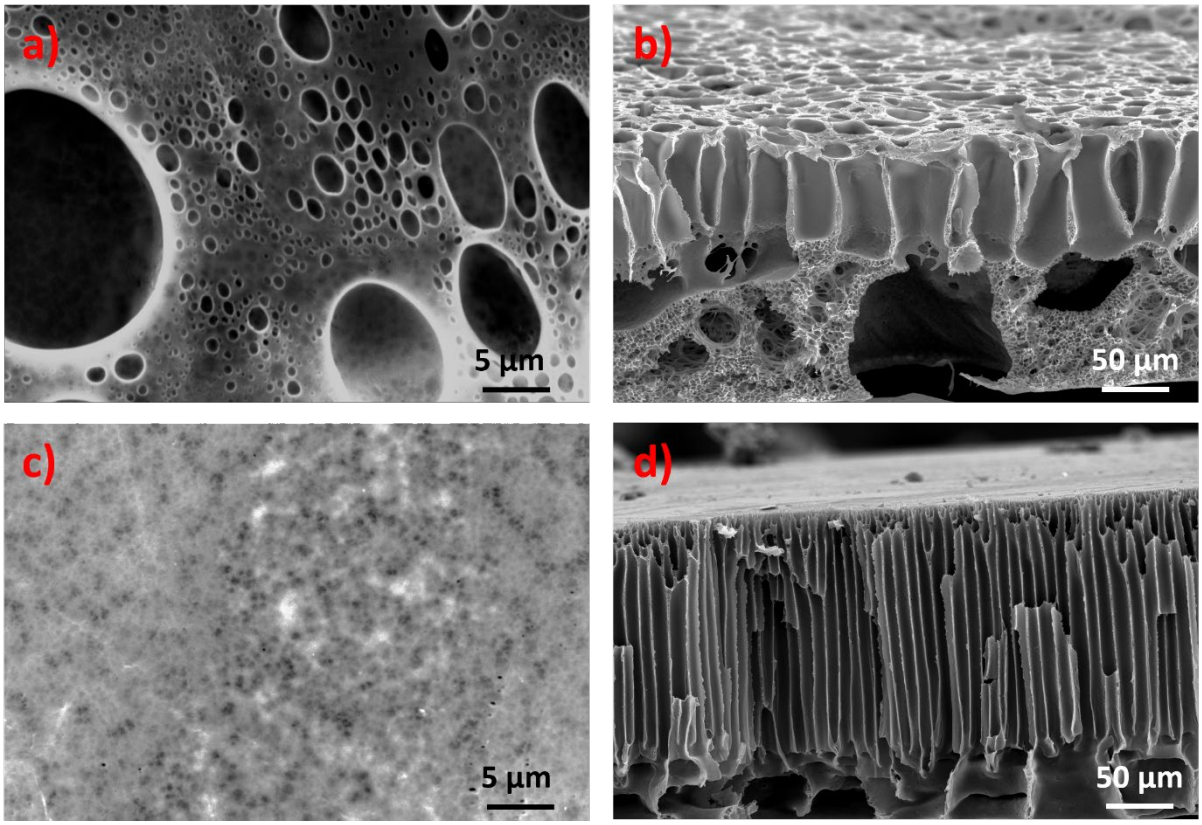

Figure 1. Surface morphologies of PES structures fabricated by NIPS triggered by (a) spray-assist technique and (c) water bath immersion. Cross section of PES structures fabricated by NIPS triggered by (b) spray-assist technique and (d) water bath immersion.

3.2 Chemical structure of TFC membranes as a function of spray cycles.

Here in this work, we deposited the selective polyamide layer on to the surface of the PES support layer *via* two methods – the traditional approach of dip coating, and our technique of spray-assisted interfacial polymerization using an automated spray coating machine. Regardless of approach used, the deposition of selective layer took place in less than 20 mins. ATR-FTIR was performed to determine the chemical composition of all TFC membranes (Fig. 2). The characteristics bands of pristine PES porous support were centered at 1485 and 1577 cm^{-1} (benzene rings), 1320 cm^{-1} (C-SO_2-C), 1148 cm^{-1} (SO_2) and 1104 cm^{-1} (C-O-C) [47-49]. After the first polyamide deposition cycle, we observed the presence of new peaks centered at 1656, 1609 and 1538 cm^{-1}. These peaks corresponded to amide II, aromatic amide and amide I structures, respectively [50]; indicating the formation of polyamide after one deposition cycle. The intensities of these amide-related peaks were relatively low when compared to the intensity

of bands of characteristic to PES porous support. As the number of deposition cycles increased from one to five, we observed that the amide-related peaks overlapped with the benzene peak of PES at 1577 cm^{-1} and the relative intensities of both C-SO_2-C and SO_2 peaks centered at 1320 cm^{-1} and 1148 cm^{-1} were lower than those of amide-related peaks. This indicated that the PES porous support layer was fully covered by polyamide after five deposition cycles. This was similar to changes in FTIR spectra as a function of deposition repetition reported previously [22].

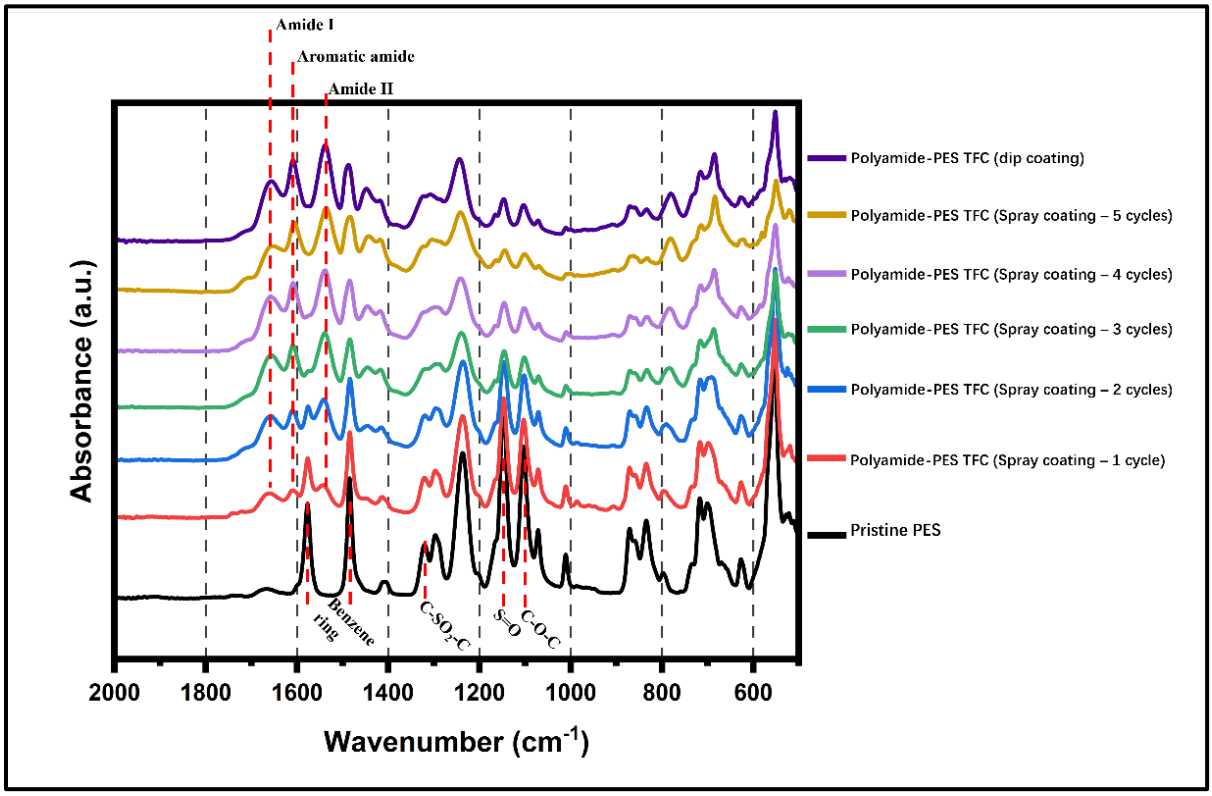

Figure 2. FTIR spectra of pristine PES porous support (black), polyamide TFC membranes fabricated with one (red), two (blue), three (green), four (purple) and five (yellow) spray cycles of polyamide deposition, and by dip coating (dark purple).

We also determined the elemental composition and chemical binding information in polyamide TFC membranes studied here from XPS survey and high-resolution scans, respectively. The atomic percentages of oxygen, carbon and nitrogen in these membranes were determined using survey scans (Table 1). Theoretically, the O/N ratio of a fully crosslinked polyamide with 100 % crosslinking degree is 1, while a fully linear polyamide chain with 0 % crosslinking degree is 2

[51]. The O/N ratio of the polyamide selective layer fabricated using n-hexane as the organic solvent *via* the conventional approach of dip coating was 1.35, indicating a crosslinking degree of 55.5 %. As TMC concentration was increased to 3 wt.% for spray-assisted deposition of CPME-based solutions, with one cycle of MPD and TMC deposition, the atomic composition of resultant polyamide film was more similar to that of a pristine PES membrane [52]. The O content was highest amongst all samples here (18.1 %), probably due to the O=S=O functional group in PES and C=O group in polyamide. This indicated that the first layer of polyamide did not fully cover the PES porous support. This was validated with SEM in the next section. Subsequent deposition of polyamide on to the initial polyamide layer yielded an O/N ratio of 1.19 and crosslinking degree of 74.4 %. The O/N ratio was reduced from 1.19 to 1.13 after the fifth deposition cycle and the crosslinking degree reached a value of 82.0 %. The reductions in O/N ratio and increments in crosslinking degree could be ascribed to prolonged reaction time as spray deposition cycles increased from two to five. This was similar to trends reported elsewhere when prolonged reaction duration enhanced crosslinking degree that also led to an increase in polyamide layer thickness [53].

Table 1. Atomic percentages, O/N ratio and crosslinking degree of TFC membranes studied here in this work.

Polyamide type	Number of spray cycles	Atomic composition			O/N ratio	Crosslinking degree
		C	N	O		
Conventional dip coating	0	74.6	10.8	14.6	1.35	55.5 %
Spray coating	1	76.6	5.36	18.1	3.38	--
	2	76.6	10.7	12.7	1.19	74.4 %
	3	76.9	10.7	12.4	1.16	77.7 %
	4	77.6	10.4	11.9	1.14	80 %
	5	77.0	10.8	12.2	1.13	82 %

The XPS survey scans and C 1s high-resolution scans (Fig. S2 and S3) further confirmed the formation of polyamide *via* conventional dip coating and our spray-assist techniques. After deconvolution of the C 1s high-resolution scans of polyamides studied here, we observed four peaks (Fig. S3) centered at 288.5 eV, 287.9 eV, 285.6 eV and 284.6 eV. These peaks could be ascribed to O=C-O, O=C-N, C-N and C-C/C-H, respectively [54, 55]. The positions of these peaks were not affected by solvent choice and fabrication technique. However, the content of each species varied as a function of crosslinking degree i.e., fabrication technique across all polyamide samples studied here. According to Scheme 1, O=C-N group was introduced by the amide forming reaction between acyl chloride in TMC and amine groups in MPD, O=C-O group was formed by hydrolysis of unreacted acyl chlorides in TMC monomers. With a crosslinking degree of 55.5 %, polyamides fabricated by dip-coating using n-hexane contained 5.7 % C=O-O and 8.9 % O=C-N. As crosslinking degree increased to 82.0 % in polyamide fabricated from five cycles of spray-assisted deposition using CPME, this polyamide only contained 1.5 % of C=O-O and 10.7 % of C=O-N. This indicated that spray-coated polyamide was more crosslinked than dip-coated polyamide. The higher crosslinking degree in spray-coated polyamide could be attributed to the use of CPME as organic solvent [32], as CPME is more soluble in water when compared to n-hexane and the required use of more TMC in CPME to yield dense, selective polyamide films [40, 54, 56].

3.3 Surface morphology of TFC membranes fabricated by spray coating.

We observed that the polyamide layer fabricated *via* dip-coating using n-hexane comprised of crumpled ridges and valleys (Fig. S4), the thickness of this polyamide layer was around 250 nm. This ridge-valley structure could be attributed to the uneven distribution of interfacial polymerization reaction heat [17, 57]. Switching to our spray-assisted technique, when water-MPD droplets and CPME-TMC droplets encountered each other on the PES porous support

layer, a thin polyamide film was formed in a confined area between the bulk water droplet and bulk organic droplet. This narrow interface layer is favorable for suppressing the polyamide layer from growing thicker and the limited amount of reactants in each droplet provided precise control of the diffusion and reaction behaviors [58]. As CPME was used as organic phase here in this study, its higher water solubility and lower interfacial tension (when compared to n-hexane) can promote MPD diffusion into the reaction zone, allowing faster thin film formation [59]. Similar results was reported when using acetone-hexane co-solvent as organic phase [60]. The resultant thinner and more lose polymer structure is favorable to higher permanence [61].

We also attempted to reduce the amount of TMC required in interfacial polymerization. With only 1 wt.% TMC in CPME, the surface pores of PES support layers could not be fully covered even with 4 deposition cycles and the surface of the resultant polyamide layer contained cracks (Fig. S5). With 5 deposition cycles, we could still observe surface cracks on the top of the selective polyamide layer. Although the 5 – 10 μm PES surface pores were covered by the polyamide layer, the surface of this polyamide layer was porous and contained < 100 nm pores. These pores might lead to low rejection rates. The reason for such porous polyamide is the insufficient TMC in CPME solution. We showed that 3 wt.% of TMC is required to yield dense selective polyamide films when CPME was used as the organic phase in our previous work [32].

When TMC concentration in CPME was increased to 3 wt.%, we observed that the surface pores of the porous PES support layer were not fully covered after one polyamide deposition cycle (Fig. 3a-b). Polyamide accumulated around the edge of the surface pores and the thicknesses of this polyamide structures were ~100 nm. With two deposition cycles, we observed the formation of the ridges and valleys structure of polyamide that fully covered the surface pores. The thickness of this polyamide layer was ~180 nm. The ridges and valleys

structures were refined after three and four cycles of polyamide deposition, while polyamide film thickness increased to ~ 250 – 380 nm (Fig. 3), similar to observations elsewhere with both large ridges and valley structure and globular projections [22]. Interestingly, here we also observed the formation of partially hollow polyamide layers after three to four cycles of polyamide deposition. Such polyamide structures are characteristic of enhanced water-organic phase dissolution rates that accelerate MPD diffusion [40, 62], and those formed by electrospraying technique [21]. Similar layer thickness increment was also reported previously using layer-by-layer interfacial polymerization method, and such hollow and sack-like structure is favorable for permeance increment [22, 63]. With five polyamide deposition cycles, the thickness of the resultant polyamide layer reached 550 nm (Fig. 3j). This could attribute to longer reaction durations and more monomeric reactants deposition [53].

Apart from tailoring surface morphology of TFC membranes, here we also observed that spray-assisted interfacial polymerization also impacted on surface roughness of polyamide selective layers (Figures 4 and S6). The surface roughness (root mean square, RMS) of the pristine PES porous support layer was 180.1 nm (Fig. 4a). The sizes and structures of surface PES pores were similar to those observed in SEM (Fig. 2a). When a polyamide layer was deposited on top of the PES porous support layer using the conventional method of dip-coating and n-hexane as the organic phase, the surface roughness of the resultant polyamide-TFC membrane was reduced to 59.99 nm (Fig. S6), similar to reports elsewhere [64, 65].

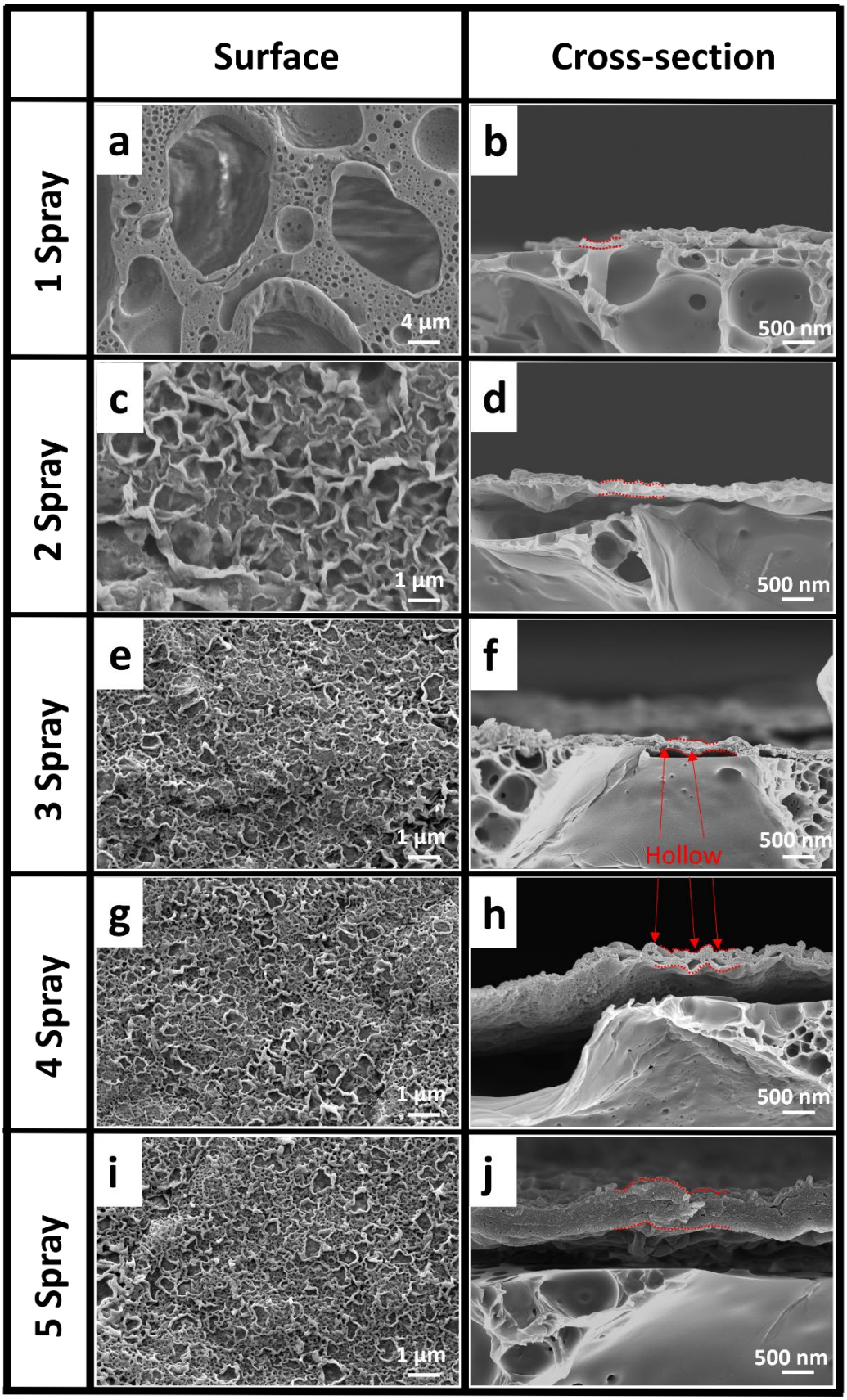

Figure 3. SEM images of TFC membranes fabricated via spray-assist method, surface scan shown on the left-hand side and cross-sectional scan shown on the rigth-hand side. a, b) 1 Spray; c, d) 2 Sprays; e, f) 3 Sprays; g, h) 4 Sprays; i, j) 5 Sprays.

1

After one cycle of spray-assisted polyamide deposition, the surface roughness was only reduced by 17.2 %, to 149.2 nm. As observed in SEM micrographs, the large pores (<5 μm) of the PES porous support layer were not fully covered by the polyamide layer. With two cycles of polyamide deposition, the surface of the PES support layer was fully covered by polyamide (Fig. 3c and 4c). This reduced the surface roughness by 75.4 %, to 44.22 nm. The surface roughness of polyamide TFC membranes increased by 13.5 %, to 50.21 nm, with five polyamide deposition cycles. Chowdhury *et al.* reported similar thicken polyamide layer formed by electrospraying technique, in their result, each layer of polyamide film cannot attach to the previous layer perfectly and will create hollow structures within different layers, which then increase the surface roughness as the number of scans increased [21]. Similar increases in surface roughness were also observed in polyamide selective layers fabricated by molecular layer-by-layer assembly [20]. Here it is important to highlight that although the surface roughness of spray coated polyamide membranes increased from 44.22 nm to 50.21 nm after 2 – 5 cycles of deposition, the overall surface roughness of our spray-coated polyamide membranes was still 16 – 26 % lower than that of dip-coated variants (59.99 nm). This reduction in surface roughness could potentially prolong the typical lifespan of such membranes (2 – 4 years) [66]. This is because reducting membrane surface roughness can mitigate fouling [67-71] and consequently enhance membrane lifespan [72, 73].

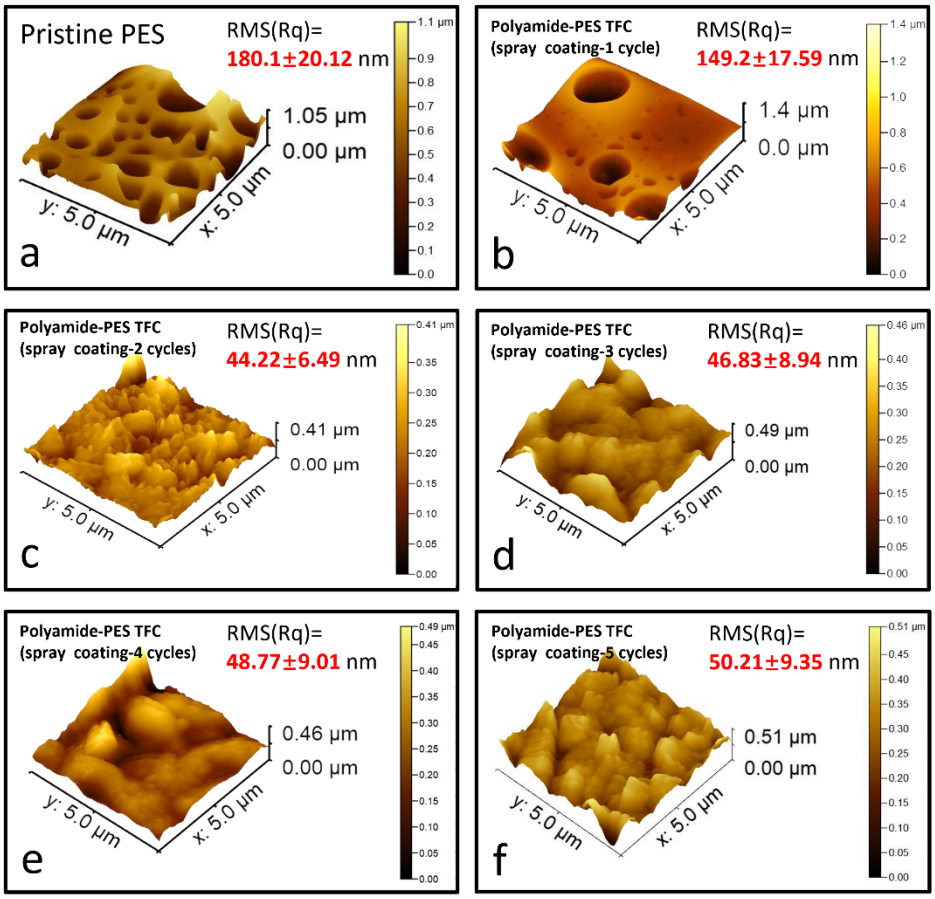

Figure 4. AFM images of all TFC membranes fabricated *via* a) conventional method and b-f) spray assist method, spray cycle increased from b) 1 spray to f) 5 sprays.

3.3 Desalination performance of all TFC membranes.

TFC membranes comprising a fully aromatic polyamide selective layer fabricated using MPD and TMC are mostly deployed for desalination [65]. The separation performances of such TFC membranes are dependent on surface morphology, chemical composition and roughness [17, 21, 65]. In this study, we tested polyamide TFC membranes that were fabricated by spray coating and dip coating against 2000 ppm NaCl water solution at 4 bar pressure. The water permeance and NaCl rejection rate of the polyamide TFC membrane fabricated *via* dip coating using n-hexane reached 1.71 L m^{-2} h^{-1} bar^{-1} and 92.3 % (Figure 5), similar to membranes fabricated from this approach reported elsewhere [31]. Meanwhile, the water permeance of polyamide membranes fabricated with CPME and dip-coating reached 1.51 L m^{-2} h^{-1} bar^{-1} and

the NaCl rejection rate was increased to 97.8 % [32]. The use of CPME as a solvent for IP via dip-coating reduced the permeance of resultant TFCs by 11.7 % whilst enhancing NaCl rejection by 5.5% [32]. This reduction in permeance and increment in NaCl rejection was ascribed to higher crosslinking degrees and thicker selective layer [74, 75], in membranes produced in CPME (79.9 % crosslinking degree and ~500 nm thickness). The crosslinking degree in dip-coated membranes fabricated with n-hexane was only 52.4 %, with a thickness of ~250 nm. When switching to spray-assist method, the water permeance and NaCl rejection rate of a TFC membrane fabricated with one polyamide deposition cycle using 1 wt.% TMC in CPME reached 9.13 L m^{-2} h^{-1} bar^{-1} and 12.5 %. With five polyamide deposition cycles, the water permeance and NaCl rejection rate of such membranes reached 5.17 L m^{-2} h^{-1} bar^{-1} and 32.1 % (Table S1). This high permeance and low rejection were mainly due to the defective selective layer (Fig. S5).

When using 3 wt.% of TMC in CPME, the water permeance of a TFC membrane fabricated by one cycle of spray-assisted polyamide deposition increased to 8.84 L m^{-2} h^{-1} bar^{-1}, but its NaCl rejection rate only reached 19. 3 %. This was most possibly due to a defective selective layer that did not cover the surface pores of the PES support as shown in Figure 3 and 4. As the polyamide deposition cycles increased from two to five, the permeances of resultant membranes reduced from 2.32 L m^{-2} h^{-1} bar^{-1} to 1.48 L m^{-2} h^{-1} bar^{-1}, while the NaCl rejection rates increased from 94.4 % to 98.3 %, respectively (Fig. 5). The increase in NaCl rejection rates could be attributed to an increase in crosslinking degree, from 74.4 % to 82.0 %, and the sealing of PES surface pores with more spray-assisted polyamide deposition cycles. Meanwhile the decrease in water permeances could be ascribed to the formation of thicker selective layers [17, 76]. Similar trends were also reported for TFC membranes comprising fully aromatic polyamide selective layers fabricated *via* the molecular layer-by-layer [20] and electrospraying techniques

[21, 24]. To evaluate the long-term performance of polyamide-PES TFC with 2 cycles of deposition, we followed published protocols [77] to extend the desalination test to 8 hours. The long-term permeances of such TFC membrane averaged at 2.32 L m^{-2} h^{-1} bar^{-1} and a rejection above 94.39% (Fig S7).

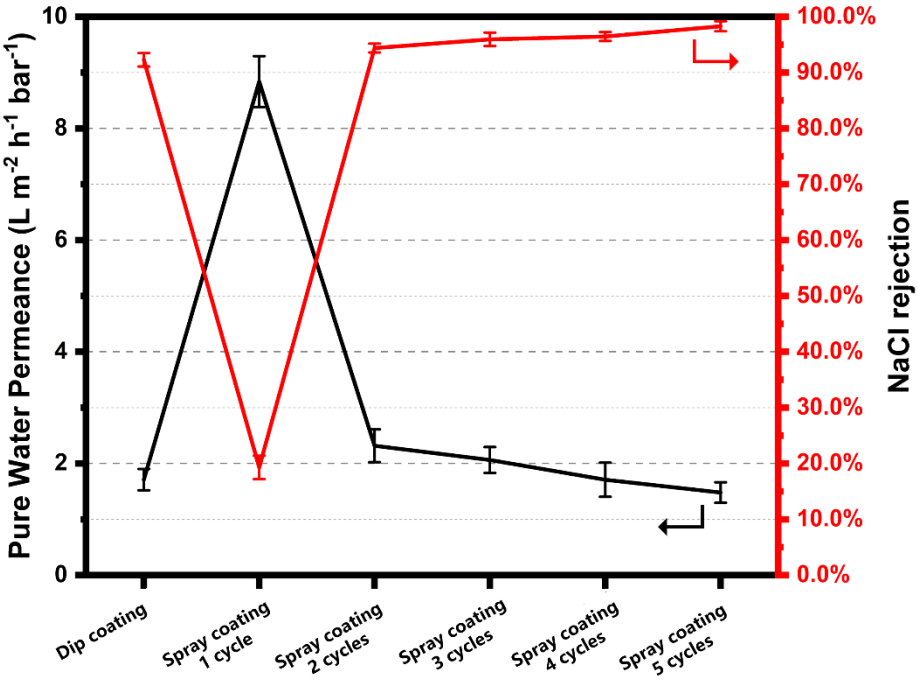

Figure 5. Pure water permeance and NaCl rejection of all membrane samples in this stuey against 2000 ppm NaCl-water solution.

Compared to the TFC membrane fabricated using dip coating and n-hexane, here we also observed that the TFC membrane fabricated from two cycles of spray-assisted polyamide deposition showed a better rejection rate of 94.4 % and a 35.7 % higher water permeance, reaching 2.32 L m^{-2} h^{-1} bar^{-1} (Table 2). Here, it is important to highlight that in current literature, the use of organic solvents other than n-hexane, for e.g., ionic liquid [78, 79], xylene or toluene [40] in interfacial polymerization typically reduced water permeance due to the increased water-organic solubility of such solvents and this would thicken the polyamide selective layer. This limitation was overcome here with the spray-assist deposition technique that alleviated the layer thickening effect associated with using solvents with improved water solubility [22, 40].

Nonetheless TFC membranes comprising MPD-TMC polyamide selective layers with sub-10 nm thickness and sub-20 nm roughness fabricated from electrospraying [21] and free interfacial polymerization [17] presented higher water permeances at 14.7 and 4.06 L m^{-2} h^{-1} bar^{-1} and similar NaCl rejection rates.

Table 2. TFC membrane RO performance comparison.

Monomer combination	IP method	Organic solvent	Rejection	Permeance (L m^{-2} h^{-1} bar^{-1})	Ref
MPD-TMC	Conventional	n-hexane	92.3%	1.71	This work
MPD-TMC	Conventional	n-hexane	90%	1.75	[80]
MPD-TMC	Conventional	Isoparrafin	95%	1.875	[79]
MPD-TMC	Conventional	Ionic liquid	98.2%	0.74	[78]
MPD-TMC	Conventional	Ionic liquid	96.8	1.09	[59]
MPD-TMC	Conventional	Xylene	99.8%	1.57	[40]
MPD-TMC	Conventional	Toluene	99.9%	1.59	[40]
MPD-TMC	Spray-assist	CPME	94.4%	2.32	This work
MPD-TMC	Electrospray	n-hexane	94%	14.7	[21]
MPD-TMC	Electrospray	n-hexane	84.7%	1.70	[24]
MPD-TMC	mLbL	Toluene	95.7%	1.39	[19]
MPD-TMC	mLbL	Toluene	98.2%	1.48	[20]
MPD-TMC	Free-interfacial	n-hexane	93.3%	4.06	[17]

4. Conclusion

In summary, in this study, we have successfully exploited the spray-assisted deposition technique to fabricate both the selective and porous support layers of a TFC membrane using

an automated spraying system. This reduced TFC membrane fabrication time from 4 days to 1 day and 40 minutes. We also showed that spray-coating can overcome the polymer thickening effect of organic solvents that are more water soluble than n-hexane that typically reduces water permeances. These findings could potentially benefit and improve the sustainability of large-scale production of polyamide TFC membranes for desalination.

Author contributions

Shiliang Lin: Conceptualization, Data curation, Formal analysis, Investigation, Methodology, Validation, Visualization, Writing-original draft and Writing-review & editing.

Yanqiu Zhang: Data curation, Formal analysis, Investigation, Methodology, Validation, and Writing-review & editing.

Lu Shao: Formal analysis, Investigation, Methodology, and Writing-review & editing.

Cher Hon Lau: Conceptualization, Formal analysis, Investigation, Methodology, Resources, Supervision, Project administration, Validation, Visualization, Writing-original draft and Writing-review & editing.

Acknowledgement

We acknowledge financial funding from the Royal Society International Exchange Grant (grant number: IECS\NSFC\201329). This work was also supported by the National Natural Science Foundation of China (22178076, 22208072).

Reference.

[1] M.M. Mekonnen, A.Y. Hoekstra, Four billion people facing severe water scarcity, Science advances 2(2) (2016) e1500323.

[2] M. Elimelech, W.A. Phillip, The Future of Seawater Desalination: Energy, Technology, and the Environment, Science 333(6043) (2011) 712-717. https://doi.org/10.1126/science.1200488.
[3] W. Yang, N. Cicek, J. Ilg, State-of-the-art of membrane bioreactors: Worldwide research and commercial applications in North America, Journal of membrane science 270(1-2) (2006) 201-211.
[4] D. Bixio, C. Thoeye, J. De Koning, D. Joksimovic, D. Savic, T. Wintgens, T. Melin, Wastewater reuse in Europe, Desalination 187(1-3) (2006) 89-101.
[5] J. Farahbakhsh, V. Vatanpour, M. Khoshnam, M. Zargar, Recent advancements in the application of new monomers and membrane modification techniques for the fabrication of thin film composite membranes: A review, Reactive and Functional Polymers 166 (2021) 105015. https://doi.org/https://doi.org/10.1016/j.reactfunctpolym.2021.105015.
[6] M.A. Shannon, P.W. Bohn, M. Elimelech, J.G. Georgiadis, B.J. Mariñas, A.M. Mayes, Science and technology for water purification in the coming decades, Nature 452(7185) (2008) 301-310. https://doi.org/10.1038/nature06599.
[7] R.H. Hailemariam, Y.C. Woo, M.M. Damtie, B.C. Kim, K.-D. Park, J.-S. Choi, Reverse osmosis membrane fabrication and modification technologies and future trends: A review, Advances in Colloid and Interface Science 276 (2020) 102100. https://doi.org/https://doi.org/10.1016/j.cis.2019.102100.
[8] A. Al-Karaghouli, L.L. Kazmerski, Energy consumption and water production cost of conventional and renewable-energy-powered desalination processes, Renewable and Sustainable Energy Reviews 24 (2013) 343-356. https://doi.org/10.1016/j.rser.2012.12.064.
[9] R. Zhang, J. Tian, S. Gao, B. Van der Bruggen, How to coordinate the trade-off between water permeability and salt rejection in nanofiltration?, Journal of Materials Chemistry A 8(18) (2020) 8831-8847. https://doi.org/10.1039/D0TA02510K.
[10] Y.S. Khoo, W.J. Lau, Y.Y. Liang, N. Yusof, A. Fauzi Ismail, Surface modification of PA layer of TFC membranes: Does it effective for performance Improvement?, Journal of Industrial and Engineering Chemistry 102 (2021) 271-292. https://doi.org/https://doi.org/10.1016/j.jiec.2021.07.006.
[11] L.E. Peng, Z. Yang, L. Long, S. Zhou, H. Guo, C.Y. Tang, A critical review on porous substrates of TFC polyamide membranes: Mechanisms, membrane performances, and future perspectives, Journal of Membrane Science 641 (2022) 119871. https://doi.org/https://doi.org/10.1016/j.memsci.2021.119871.
[12] M. Son, H.-g. Choi, L. Liu, E. Celik, H. Park, H. Choi, Efficacy of carbon nanotube positioning in the polyethersulfone support layer on the performance of thin-film composite membrane for desalination, Chemical Engineering Journal 266 (2015) 376-384. https://doi.org/https://doi.org/10.1016/j.cej.2014.12.108.
[13] A.F. Ismail, M. Padaki, N. Hilal, T. Matsuura, W.J. Lau, Thin film composite membrane — Recent development and future potential, Desalination 356 (2015) 140-148. https://doi.org/10.1016/j.desal.2014.10.042.
[14] L. Zhao, P.C.Y. Chang, C. Yen, W.S.W. Ho, High-flux and fouling-resistant membranes for brackish water desalination, Journal of Membrane Science 425-426 (2013) 1-10. https://doi.org/https://doi.org/10.1016/j.memsci.2012.09.018.
[15] J.H. Kim, M. Cook, S.H. Park, S.J. Moon, J.F. Kim, A.G. Livingston, Y.M. Lee, A compact and scalable fabrication method for robust thin film composite membranes, Green Chemistry 20(8) (2018) 1887-1898. https://doi.org/10.1039/C8GC00731D.
[16] H. Yan, X. Miao, J. Xu, G. Pan, Y. Zhang, Y. Shi, M. Guo, Y. Liu, The porous structure of the fully-aromatic polyamide film in reverse osmosis membranes, Journal of Membrane Science 475 (2015) 504-510. https://doi.org/10.1016/j.memsci.2014.10.052.

[17] Z. Jiang, S. Karan, A.G. Livingston, Water Transport through Ultrathin Polyamide Nanofilms Used for Reverse Osmosis, Adv Mater 30(15) (2018) e1705973. https://doi.org/10.1002/adma.201705973.
[18] J. Zhu, J. Hou, R. Zhang, S. Yuan, J. Li, M. Tian, P. Wang, Y. Zhang, A. Volodin, B. Van der Bruggen, Rapid water transport through controllable, ultrathin polyamide nanofilms for high-performance nanofiltration, Journal of Materials Chemistry A 6(32) (2018) 15701-15709. https://doi.org/10.1039/c8ta05687k.
[19] J.E. Gu, S. Lee, C.M. Stafford, J.S. Lee, W. Choi, B.Y. Kim, K.Y. Baek, E.P. Chan, J.Y. Chung, J. Bang, J.H. Lee, Molecular layer-by-layer assembled thin-film composite membranes for water desalination, Adv Mater 25(34) (2013) 4778-82. https://doi.org/10.1002/adma.201302030.
[20] W. Choi, J.-E. Gu, S.-H. Park, S. Kim, J. Bang, K.-Y. Baek, B. Park, J.S. Lee, E.P. Chan, J.-H. Lee, Tailor-Made Polyamide Membranes for Water Desalination, ACS Nano 9(1) (2015) 345-355. https://doi.org/10.1021/nn505318v.
[21] M.R. Chowdhury, J. Steffes, B.D. Huey, J.R. McCutcheon, 3D printed polyamide membranes for desalination, Science 361(6403) (2018) 682-686. https://doi.org/10.1126/science.aar2122.
[22] T. Tsuru, S. Sasaki, T. Kamada, T. Shintani, T. Ohara, H. Nagasawa, K. Nishida, M. Kanezashi, T. Yoshioka, Multilayered polyamide membranes by spray-assisted 2-step interfacial polymerization for increased performance of trimesoyl chloride (TMC)/m-phenylenediamine (MPD)-derived polyamide membranes, Journal of Membrane Science 446 (2013) 504-512. https://doi.org/10.1016/j.memsci.2013.07.031.
[23] J.B. Schlenoff, S.T. Dubas, T. Farhat, Sprayed Polyelectrolyte Multilayers, Langmuir 16(26) (2000) 9968-9969. https://doi.org/10.1021/la001312i.
[24] X.-H. Ma, Z. Yang, Z.-K. Yao, H. Guo, Z.-L. Xu, C.Y. Tang, Interfacial Polymerization with Electrosprayed Microdroplets: Toward Controllable and Ultrathin Polyamide Membranes, Environmental Science & Technology Letters 5(2) (2018) 117-122. https://doi.org/10.1021/acs.estlett.7b00566.
[25] A. Izquierdo, S.S. Ono, J.C. Voegel, P. Schaaf, G. Decher, Dipping versus Spraying: Exploring the Deposition Conditions for Speeding Up Layer-by-Layer Assembly, Langmuir 21(16) (2005) 7558-7567. https://doi.org/10.1021/la047407s.
[26] H. Tang, G. Zhang, S. Ji, Rapid assembly of polyelectrolyte multilayer membranes using an automatic spray system, AIChE Journal 59(1) (2013) 250-257. https://doi.org/10.1002/aic.13810.
[27] R. Wang, L. Shan, G. Zhang, S. Ji, Multiple sprayed composite membranes with high flux for alcohol permselective pervaporation, Journal of Membrane Science 432 (2013) 33-41. https://doi.org/https://doi.org/10.1016/j.memsci.2013.01.006.
[28] J. Lin, F. Lin, R. Liu, P. Li, S. Fang, W. Ye, S. Zhao, Scalable fabrication of robust superhydrophobic membranes by one-step spray-coating for gravitational water-in-oil emulsion separation, Separation and Purification Technology 231 (2020) 115898. https://doi.org/https://doi.org/10.1016/j.seppur.2019.115898.
[29] Z. Zhou, Y. Hu, C. Boo, Z. Liu, J. Li, L. Deng, X. An, High-Performance Thin-Film Composite Membrane with an Ultrathin Spray-Coated Carbon Nanotube Interlayer, Environmental Science & Technology Letters 5(5) (2018) 243-248. https://doi.org/10.1021/acs.estlett.8b00169.
[30] Y.-R. Xue, Z.-Y. Ma, C. Liu, C.-Y. Zhu, J. Wu, Z.-K. Xu, Polyamide nanofilms synthesized by a sequential process of blade coating-spraying-interfacial polymerization toward reverse osmosis, Separation and Purification Technology 310 (2023). https://doi.org/10.1016/j.seppur.2023.123122.

[31] S.L. Lin, S.S. He, S. Sarwar, R.A. Milescu, C.R. McElroy, S. Dimartino, L. Shao, C.H. Lau, Spray coating polymer substrates from a green solvent to enhance desalination performances of thin film composites, Journal of Materials Chemistry A 11(2) (2023) 891-900. https://doi.org/10.1039/d2ta07200a.
[32] S. Lin, A.C. Semiao, Y. Zhang, S. Lu, C.H. Lau, Interfacial polymerization using biobased solvents and their application as desalination and organic solvent nanofiltration membranes, Journal of Membrane Science (2023) 122281. https://doi.org/https://doi.org/10.1016/j.memsci.2023.122281.
[33] S. Zinadini, A.A. Zinatizadeh, M. Rahimi, V. Vatanpour, H. Zangeneh, Preparation of a novel antifouling mixed matrix PES membrane by embedding graphene oxide nanoplates, Journal of Membrane Science 453 (2014) 292-301. https://doi.org/https://doi.org/10.1016/j.memsci.2013.10.070.
[34] Y.J. Lim, K. Goh, G.S. Lai, Y. Zhao, J. Torres, R. Wang, Unraveling the role of support membrane chemistry and pore properties on the formation of thin-film composite polyamide membranes, Journal of Membrane Science 640 (2021) 119805. https://doi.org/https://doi.org/10.1016/j.memsci.2021.119805.
[35] F. Alibakhshian, M. Pourafshari Chenar, M. Asghari, M.R. Moradi, Layer-by-layer polyamide thin film nanocomposite membrane: synthesis, characterization and using as pervaporation membrane to separate methyl tertiary butyl ether/methanol mixture, Journal of Polymer Research 28(4) (2021) 116. https://doi.org/10.1007/s10965-021-02479-0.
[36] M.J. Park, C. Wang, R.R. Gonzales, S. Phuntsho, H. Matsuyama, E. Drioli, H.K. Shon, Fabrication of thin film composite polyamide membrane for water purification via inkjet printing of aqueous and solvent inks, Desalination 541 (2022) 116027. https://doi.org/https://doi.org/10.1016/j.desal.2022.116027.
[37] Y. Wang, R. Ou, Q. Ge, H. Wang, T. Xu, Preparation of polyethersulfone/carbon nanotube substrate for high-performance forward osmosis membrane, Desalination 330 (2013) 70-78. https://doi.org/https://doi.org/10.1016/j.desal.2013.09.028.
[38] Y. Ono, Y. Takeuchi, N. Hisanaga, A comparative study on the toxicity of n-hexane and its isomers on the peripheral nerve, International Archives of Occupational and Environmental Health 48(3) (1981) 289-294. https://doi.org/10.1007/BF00405616.
[39] D.J. Lanska, Limitations of Occupational Air Contaminant Standards, as Exemplified by the Neurotoxin N-hexane, Journal of Public Health Policy 20(4) (1999) 441-458. https://doi.org/10.2307/3343130.
[40] S.-J. Park, S.J. Kwon, H.-E. Kwon, M.G. Shin, S.-H. Park, H. Park, Y.-I. Park, S.-E. Nam, J.-H. Lee, Aromatic solvent-assisted interfacial polymerization to prepare high performance thin film composite reverse osmosis membranes based on hydrophilic supports, Polymer 144 (2018) 159-167. https://doi.org/10.1016/j.polymer.2018.04.060.
[41] S. Yang, J. Wang, Y. Wang, Y. Ding, W. Zhang, F. Liu, Interfacial polymerized polyamide nanofiltration membrane by demulsification of hexane-in-water droplets through hydrophobic PTFE membrane: Membrane performance and formation mechanism, Separation and Purification Technology 275 (2021). https://doi.org/10.1016/j.seppur.2021.119227.
[42] Y. Li, X. You, R. Li, Y. Li, C. Yang, M. Long, R. Zhang, Y. Su, Z. Jiang, Loosening ultrathin polyamide nanofilms through alkali hydrolysis for high-permselective nanofiltration, Journal of Membrane Science 637 (2021). https://doi.org/10.1016/j.memsci.2021.119623.
[43] A. Soroush, J. Barzin, M. Barikani, M. Fathizadeh, Interfacially polymerized polyamide thin film composite membranes: Preparation, characterization and performance evaluation, Desalination 287 (2012) 310-316. https://doi.org/https://doi.org/10.1016/j.desal.2011.07.048.
[44] A. Rahimpour, S.S. Madaeni, S. Ghorbani, A. Shockravi, Y. Mansourpanah, The influence of sulfonated polyethersulfone (SPES) on surface nano-morphology and

performance of polyethersulfone (PES) membrane, Applied Surface Science 256(6) (2010) 1825-1831. https://doi.org/https://doi.org/10.1016/j.apsusc.2009.10.014.
[45] L. Marbelia, A. Ilyas, M. Dierick, J. Qian, C. Achille, R. Ameloot, I.F.J. Vankelecom, Preparation of patterned flat-sheet membranes using a modified phase inversion process and advanced casting knife construction techniques, Journal of Membrane Science 597 (2020). https://doi.org/10.1016/j.memsci.2019.117621.
[46] A. Ilyas, M. Mertens, S. Oyaert, I.F.J. Vankelecom, Synthesis of patterned PVDF ultrafiltration membranes: Spray-modified non-solvent induced phase separation, Journal of Membrane Science 612 (2020). https://doi.org/10.1016/j.memsci.2020.118383.
[47] C.-C. Ho, J.F. Su, L.-P. Cheng, Fabrication of high-flux asymmetric polyethersulfone (PES) ultrafiltration membranes by nonsolvent induced phase separation process: Effects of H2O contents in the dope, Polymer : the International journal for the Science and Technology of polymers. 217 (2021) 123451. https://doi.org/10.1016/j.polymer.2021.123451.
[48] M.J. Luján-Facundo, J.A. Mendoza-Roca, B. Cuartas-Uribe, S. Álvarez-Blanco, Evaluation of cleaning efficiency of ultrafiltration membranes fouled by BSA using FTIR–ATR as a tool, Journal of Food Engineering 163 (2015) 1-8. https://doi.org/10.1016/j.jfoodeng.2015.04.015.
[49] R.A. Milescu, C.R. McElroy, T.J. Farmer, P.M. Williams, M.J. Walters, J.H. Clark, Fabrication of PES/PVP Water Filtration Membranes Using Cyrene®, a Safer Bio-Based Polar Aprotic Solvent, Advances in Polymer Technology 2019 (2019) 1-15. https://doi.org/10.1155/2019/9692859.
[50] B. Khorshidi, T. Thundat, B.A. Fleck, M. Sadrzadeh, Thin film composite polyamide membranes: parametric study on the influence of synthesis conditions, RSC Advances 5(68) (2015) 54985-54997. https://doi.org/10.1039/c5ra08317f.
[51] P.M. Johnson, J. Yoon, J.Y. Kelly, J.A. Howarter, C.M. Stafford, Molecular layer‐by‐layer deposition of highly crosslinked polyamide films, Journal of Polymer Science Part B: Polymer Physics 50(3) (2011) 168-173. https://doi.org/10.1002/polb.23002.
[52] S.X. Liu, J.-T. Kim, Characterization of Surface Modification of Polyethersulfone Membrane, Journal of Adhesion Science and Technology 25(1-3) (2012) 193-212. https://doi.org/10.1163/016942410x503311.
[53] S. Habib, S.T. Weinman, A review on the synthesis of fully aromatic polyamide reverse osmosis membranes, Desalination 502 (2021). https://doi.org/10.1016/j.desal.2021.114939.
[54] X. Wei, Y. Peng, W. Fang, Z. Hu, W. Li, S. Zhang, J. Jin, A polyaniline nanofiber array supported ultrathin polyamide membrane for solar-driven volatile organic compound removal, Journal of Materials Chemistry A 10(38) (2022) 20424-20430. https://doi.org/10.1039/d2ta04909k.
[55] Z. Zhang, G. Kang, H. Yu, Y. Jin, Y. Cao, From reverse osmosis to nanofiltration: Precise control of the pore size and charge of polyamide membranes via interfacial polymerization, Desalination 466 (2019) 16-23. https://doi.org/10.1016/j.desal.2019.05.001.
[56] M. Shan, H. Kang, Z. Xu, N. Li, M. Jing, Y. Hu, K. Teng, X. Qian, J. Shi, L. Liu, Decreased cross-linking in interfacial polymerization and heteromorphic support between nanoparticles: Towards high-water and low-solute flux of hybrid forward osmosis membrane, J Colloid Interface Sci 548 (2019) 170-183. https://doi.org/10.1016/j.jcis.2019.04.014.
[57] I. Nulens, R. Peters, R. Verbeke, D.M. Davenport, C. Van Goethem, B. De Ketelaere, P. Goos, K.V. Agrawal, I.F.J. Vankelecom, MPD and TMC supply as parameters to describe synthesis-morphology-performance relationships of polyamide thin film composite membranes, Journal of Membrane Science 667 (2023). https://doi.org/10.1016/j.memsci.2022.121155.

[58] L. Shan, J. Gu, H. Fan, S. Ji, G. Zhang, Microphase Diffusion-Controlled Interfacial Polymerization for an Ultrahigh Permeability Nanofiltration Membrane, ACS Appl Mater Interfaces 9(51) (2017) 44820-44827. https://doi.org/10.1021/acsami.7b14017.
[59] H. Marien, L. Bellings, S. Hermans, I.F. Vankelecom, Sustainable Process for the Preparation of High-Performance Thin-Film Composite Membranes using Ionic Liquids as the Reaction Medium, ChemSusChem 9(10) (2016) 1101-11. https://doi.org/10.1002/cssc.201600123.
[60] C. Kong, M. Kanezashi, T. Yamomoto, T. Shintani, T. Tsuru, Controlled synthesis of high performance polyamide membrane with thin dense layer for water desalination, Journal of Membrane Science 362(1) (2010) 76-80. https://doi.org/https://doi.org/10.1016/j.memsci.2010.06.022.
[61] C. Kong, T. Shintani, T. Kamada, V. Freger, T. Tsuru, Co-solvent-mediated synthesis of thin polyamide membranes, Journal of Membrane Science 384(1) (2011) 10-16. https://doi.org/https://doi.org/10.1016/j.memsci.2011.08.055.
[62] T. Kamada, T. Ohara, T. Shintani, T. Tsuru, Optimizing the preparation of multi-layered polyamide membrane via the addition of a co-solvent, Journal of Membrane Science 453 (2014) 489-497. https://doi.org/https://doi.org/10.1016/j.memsci.2013.11.028.
[63] W. Choi, S. Jeon, S.J. Kwon, H. Park, Y.-I. Park, S.-E. Nam, P.S. Lee, J.S. Lee, J. Choi, S. Hong, E.P. Chan, J.-H. Lee, Thin film composite reverse osmosis membranes prepared via layered interfacial polymerization, Journal of Membrane Science 527 (2017) 121-128. https://doi.org/10.1016/j.memsci.2016.12.066.
[64] H. Hoseinpour, M. Peyravi, A. Nozad, M. Jahanshahi, Static and dynamic assessments of polysulfonamide and poly(amide-sulfonamide) acid-stable membranes, Journal of the Taiwan Institute of Chemical Engineers 67 (2016) 453-466. https://doi.org/10.1016/j.jtice.2016.07.039.
[65] C.Y.Y. Tang, Y.N. Kwon, J.O. Leckie, Effect of membrane chemistry and coating layer on physiochemical properties of thin film composite polyamide RO and NF membranes I. FTIR and XPS characterization of polyamide and coating layer chemistry, Desalination 242(1-3) (2009) 149-167. https://doi.org/10.1016/j.desal.2008.04.003.
[66] L. Le Petit, M. Rabiller-Baudry, R. Touin, R. Chataignier, P. Thomas, O. Connan, R. Périon, Efficient and rapid multiscale approach of polymer membrane degradation and stability: Application to formulation of harmless non-oxidative biocide for polyamide and PES/PVP membranes, Separation and Purification Technology 259 (2021) 118054. https://doi.org/https://doi.org/10.1016/j.seppur.2020.118054.
[67] C. Zhou, Y. Shi, C. Sun, S. Yu, M. Liu, C. Gao, Thin-film composite membranes formed by interfacial polymerization with natural material sericin and trimesoyl chloride for nanofiltration, Journal of Membrane Science 471 (2014) 381-391. https://doi.org/https://doi.org/10.1016/j.memsci.2014.08.033.
[68] Q. An, F. Li, Y. Ji, H. Chen, Influence of polyvinyl alcohol on the surface morphology, separation and anti-fouling performance of the composite polyamide nanofiltration membranes, Journal of Membrane Science 367(1) (2011) 158-165. https://doi.org/https://doi.org/10.1016/j.memsci.2010.10.060.
[69] P.H. Duong, J. Zuo, S.P. Nunes, Dendrimeric thin-film composite membranes: free volume, roughness, and fouling resistance, Industrial & Engineering Chemistry Research 56(48) (2017) 14337-14349.
[70] G.-R. Xu, J.-N. Wang, C.-J. Li, Strategies for improving the performance of the polyamide thin film composite (PA-TFC) reverse osmosis (RO) membranes: Surface modifications and nanoparticles incorporations, Desalination 328 (2013) 83-100.

[71] X. Ma, Z. Yang, Z. Yao, H. Guo, Z. Xu, C.Y. Tang, Tuning roughness features of thin film composite polyamide membranes for simultaneously enhanced permeability, selectivity and anti-fouling performance, Journal of colloid and interface science 540 (2019) 382-388.
[72] K.O. Agenson, T. Urase, Change in membrane performance due to organic fouling in nanofiltration (NF)/reverse osmosis (RO) applications, Separation and Purification Technology 55(2) (2007) 147-156.
[73] S. Al Aani, C.J. Wright, N. Hilal, Investigation of UF membranes fouling and potentials as pre-treatment step in desalination and surface water applications, Desalination 432 (2018) 115-127.
[74] K. Chen, P. Li, H. Zhang, H. Sun, X. Yang, D. Yao, X. Pang, X. Han, Q. Jason Niu, Organic solvent nanofiltration membrane with improved permeability by in-situ growth of metal-organic frameworks interlayer on the surface of polyimide substrate, Separation and Purification Technology 251 (2020) 117387.
https://doi.org/https://doi.org/10.1016/j.seppur.2020.117387.
[75] X. Zhang, T. Li, Z. Wang, J. Wang, S. Zhao, Polar aprotic solvent-resistant nanofiltration membranes generated by flexible-chain binding interfacial polymerization onto PTFE substrate, Journal of Membrane Science 668 (2023) 121294.
https://doi.org/https://doi.org/10.1016/j.memsci.2022.121294.
[76] Y. Cui, X.-Y. Liu, T.-S. Chung, Ultrathin Polyamide Membranes Fabricated from Free-Standing Interfacial Polymerization: Synthesis, Modifications, and Post-treatment, Industrial & Engineering Chemistry Research 56(2) (2017) 513-523.
https://doi.org/10.1021/acs.iecr.6b04283.
[77] B.-Q. Huang, Z.-L. Xu, H. Ding, M.-C. Miao, Y.-J. Tang, Antifouling sulfonated polyamide nanofiltration hollow fiber membrane prepared with mixed diamine monomers of BDSA and PIP, RSC Advances 7(89) (2017) 56629-56637.
https://doi.org/10.1039/C7RA11632B.
[78] Y. Hartanto, M. Corvilain, H. Mariën, J. Janssen, I.F.J. Vankelecom, Interfacial polymerization of thin-film composite forward osmosis membranes using ionic liquids as organic reagent phase, Journal of Membrane Science 601 (2020) 117869.
https://doi.org/https://doi.org/10.1016/j.memsci.2020.117869.
[79] Z. Yong, Y. Sanchuan, L. Meihong, G. Congjie, Polyamide thin film composite membrane prepared from m-phenylenediamine and m-phenylenediamine-5-sulfonic acid, Journal of Membrane Science 270(1) (2006) 162-168.
https://doi.org/https://doi.org/10.1016/j.memsci.2005.06.053.
[80] H. Zhao, S. Qiu, L. Wu, L. Zhang, H. Chen, C. Gao, Improving the performance of polyamide reverse osmosis membrane by incorporation of modified multi-walled carbon nanotubes, Journal of Membrane Science 450 (2014) 249-256.
https://doi.org/https://doi.org/10.1016/j.memsci.2013.09.014.